Hindawi Publishing Corporation
Mathematical Problems in Engineering
Volume 2014, Article ID 287076, 11 pages
http://dx.doi.org/10.1155/2014/287076

Research Article

Loading and Contact Stress Analysis on the Thread Teeth in Tubing and Casing Premium Threaded Connection

Honglin Xu,[1] Taihe Shi,[1] Zhi Zhang,[1] and Bin Shi[2]

[1] *State Key Laboratory of Oil and Gas Reservoir Geology and Exploitation, School of Petroleum and Natural Gas Engineering, Southwest Petroleum University, Chengdu 610500, China*
[2] *R&D Center of Tianjin Pipe (Group) Corporation, Ltd., Tianjin 300301, China*

Correspondence should be addressed to Honglin Xu; xuhlaca1986_jy@163.com

Received 20 April 2014; Revised 15 August 2014; Accepted 21 August 2014; Published 13 October 2014

Academic Editor: Chunlin Chen

Copyright © 2014 Honglin Xu et al. This is an open access article distributed under the Creative Commons Attribution License, which permits unrestricted use, distribution, and reproduction in any medium, provided the original work is properly cited.

Loading and contact stress distribution on the thread teeth in tubing and casing premium threaded connections are of great importance for design optimization, pretightening force control, and thread failure prevention. This paper proposes an analytical method based on the elastic mechanics. This is quite different from other papers, which mainly rely on finite element analysis. The differential equation of load distribution on the thread teeth was established according to equal pitch of the engaged thread after deformation and solved by finite difference method. Furthermore, the relation between load acting on each engaged thread and mean contact stress on its load flank is set up based on the geometric description of thread surface. By comparison, this new analytical method with the finite element analysis for a modified API 177.8 mm premium threaded connection is approved. Comparison of the contact stress on the last engaged thread between analytical model and FEM shows that the accuracy of analytical model will decline with the increase of pretightening force after the material enters into plastic deformation. However, the analytical method can meet the needs of engineering to some extent because its relative error is about 6.2%~18.1% for the in-service level of pretightening force.

1. Introduction

Premium threaded connections have been widely used for maintaining structural and sealing integrity of tubing and casing strings in HPHT wells. The overwhelming majority of premium threaded connections are characterized by a tapered metal-to-metal seal structure for leakage resistance and an interior rotary torque shoulder to control final make-up torques, providing additional sealing performance (shown in Figure 1). These characteristics are different from API buttress thread connections and extreme-line thread connections [1–3]. In general, the thread teeth of premium threaded connection are used to bear axial tensile load, due to the load flank angle α design (shown in Figure 3) of usually $-4^\circ\sim3^\circ$. We also noticed that the taper angle of metal-to-metal seal is usually $1.79^\circ\sim2.86^\circ$, so the axial component of sealing contact stress could be neglected and the action force of sealing and shoulder replaced approximatively by an axial pretightening force F_t acting on the A-B cross section plane (shown in Figure 1). Consequently, it is significant to investigate the load and contact stress on thread teeth caused by this pretightening force F_t for design optimization, pretightening torque control, and thread failure prevention.

The load distribution and contact stress on thread teeth were investigated in many previous references in the last century, whose methods can mainly be divided into three categories. The first category is developed on the basis of analytical method. Maduschka [4] and Sopwith [5] first proposed the models of the load distribution in cylindrical screw threads, whose results clearly indicate that the first three or four engaged threads carry more than half of the preload induced by the make-up torque. Taking axial and tangential forces, as well as bending moments, into consideration, Yazawa and Hongo [6] developed a model to investigate the load distribution of a bolt-nut connection. Wang and Marshek [7] also established a spring model to predict the load distribution of bolt-nut connection. Furthermore, Bruschelli and Latorrata [8] developed an analytical model to

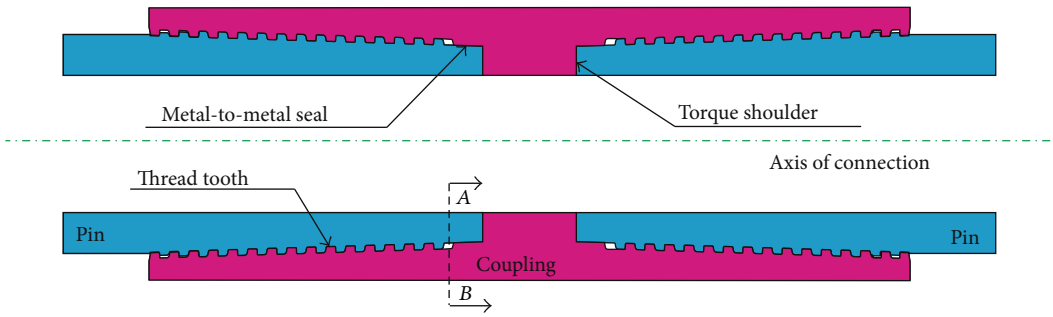

Figure 1: The schematic of a premium threaded connection.

study the load distribution for conical threads connections. Chen et al. [9] presented a practical and convenient model for cylindrical pipe threaded connection, which can be applied to calculate the load and deformation on each thread tooth just with tightening torque and thread numbers. The vast majority of the analytical models mentioned above are established from screw threaded connection or cylindrical pipe threaded connection and therefore are not applicable to premium connection: its tapered thread connection type contains special metal-to metal seal, interior rotary torque shoulder, and the specialized tooth form of buttress.

The second category method is developed based on finite element method (FEM). Capable of considering material nonlinear behavior and complex boundary conditions easily, FEM makes studying the load distribution, contact stress, and stress concentration on the thread tooth possible. O'Hara [10] established a 2D axisymmetric model of thread connection based on thread characteristic lengths and the numerical results were generally validated by Heywood's equations. Bretl and Cook [11] proposed a unique FEM technique for threaded connections and their simulated results agreed with those from analytical and experimental methods both for conventional and for tapered threads. Zhao [12, 13] developed an elastic-plastic FEM and investigated the load distribution and SCFs (stress concentration factors) of the bolt-nut connection. Macdonald and Deans [14] acquired the SCFs and induced stresses on the drilling string thread and they found out that the high local stresses are located at the root of the first engaged tooth in the pin and the last engaged tooth in the box. Bahai et al. [15] also calculated the SCFs of API drill string threaded connector subjected to preloading, axial loading, and bending loads. Chen and Shih [16] developed a 3D FEM for bolted joints and analyzed the helical and friction effect on the load distribution of each thread. Baragetti [17] proposed a numerical finite element procedure for rotary shouldered connections (RSCs) and quantified the effects of taper on the loads carried by each engaged thread and contact stress on the thread flanks. Fukuoka and Nomura [18] established the FE model with accurate thread geometry by deriving a mathematical expression of the helical thread geometry of a single-thread screw. The numerical results indicate that axial load along engaged threads shows a different distribution pattern from those obtained by axisymmetric FE analysis and elastic theory. Although FE models have incomparable advantages for threaded connections analysis, most of them are based on 2D axisymmetric assumptions and the helix angle is usually ignored.

The third category method is developed based on experimental testing. Stoeckly and Macke [19] developed a testing apparatus to measure the axial displacement of the threads and compare their experimental data by modifying Sopwith equations. They found out that the frictional coefficient between the lubricated bolt and nut has little effect on the thread load distribution. Yuan et al. [20] tested the make-up and break-out operations in oilfields by placing the foil gauges on the inner surface of the male thread and the outer surface of the female thread along the axial and tangential direction and concluded that those operations have a strong impact on the service life of oil tubing threaded connection. Plácido et al. [21] carried out some full and reduced scale experimental tests on aluminum drill pipes to investigate their fatigue mechanism under cyclic bending and constant tensile loads. Slack et al. [22] proposed the ultrasonic reflection techniques to directly measure the contact stress between thread and sealing surface. It turned out to be an accurate and effective method to evaluate the sealing performance and to detect sealing damage in premium connections [23]. Though experimental testing can be an effective method for validating analytical models and FEM, those tests focused on limited aspects of threaded connection problems and are difficult for application in practice.

Based on elastic mechanics theory and some simplifications, this paper proposed an analytical method to calculate the load distribution and contact stress on each engaged thread tooth for premium threaded connections. The 2D FEM validated the analytical model, and the comparison of the contact stress on the last engaged thread between two methods investigated the accuracy of the analytical model and its practicality in engineering.

2. Model Development and Solution

2.1. Loading Analysis on the Premium Threaded Connection. During tightening, the engaged threads of a premium connection will transfer the pretightening force F_t caused mainly by shoulder contact, thus leading to the compressed pin and the stretched coupling. To facilitate the analytical model, we assumed all thread teeth were intact and let

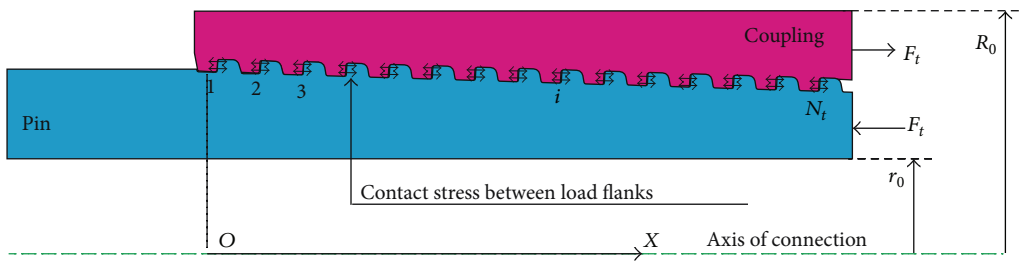

Figure 2: The schematic of load distribution for premium connection.

the axis of premium threaded connection as x direction to establish a one-dimensional coordinate system OX with itsorigin being at the big end of the pin thread. Meanwhile, the engaged thread teeth were numbered $1 \sim N_t$ consecutively from origin to the small end of the pin thread (shown in Figure 2).

The contact stresses between load flanks of engaged thread interact with each other as action and reaction, so the axial load distribution $F(x)$ along x direction is equal within pin thread and coupling thread. Let $f(x)$ denote the load distribution intensity; then

$$f(x) = \frac{\mathrm{d}F(x)}{\mathrm{d}x}. \tag{1}$$

The load distribution intensity $f(x)$ equals the axial load acting on the engaged thread within unit axial length, which reflects the distribution characteristics of pretightening force along the engaged thread. It is obvious that axial load distribution $F(x)$ can be calculated by the integral formula as follows:

$$F(x) = \int_0^x f(x)\,\mathrm{d}x. \tag{2}$$

The axial load acting on each engaged thread can be further obtained as

$$\begin{aligned} F_{iP} &= F[iP] - F[(i-1)P] \\ &= \int_{(i-1)P}^{iP} f(x)\,\mathrm{d}x, \quad (i = 1, 2, \ldots, N_t). \end{aligned} \tag{3}$$

2.2. Deformation of Thread Tooth in Premium Threaded Connection. The thread tooth profile of most premium connections typically adopts modified API buttress type thread, whose deformation can be calculated by simplifying itself into a cantilever beam model of an isosceles trapezoid [24] (shown in Figure 3).

The necessary parameters for calculating the elastic deformation of simplified thread tooth can be obtained from this basic geometry parameter of buttress type thread:

$$\begin{aligned} a &= \frac{P - F_{\mathrm{rs}}}{\cos\gamma}, \\ b &= a - c\left[\tan(\alpha - \gamma) + \tan(\beta + \gamma)\right], \\ c &= \frac{h_B \cos\gamma}{2}. \end{aligned} \tag{4}$$

According to [24], the deformations of simplified thread tooth are mainly caused by five reasons (shown in Figure 4). Now, let angle $\alpha - \gamma$ be equal to ϑ in Figure 4, and the thread tooth deformation δ_a caused by tooth bending can be expressed as

$$\begin{aligned} \delta_a(x) = {} & \frac{N(x)\cos(\alpha-\gamma)}{E}\frac{3(1-\nu^2)}{4} \\ & \cdot \left\{\left[1 - \left(2 - \frac{b}{a}\right)^2 + 2\ln\left(\frac{a}{b}\right)\right] c\tan^3(\alpha-\gamma) \right. \\ & \left. - 4\left(\frac{c}{a}\right)^2 \tan(\alpha-\gamma)\right\}. \end{aligned} \tag{5}$$

The thread tooth deformation δ_b caused by shear force can be expressed as

$$\begin{aligned} & \delta_b(x) \\ & = \frac{N(x)\cos(\alpha-\gamma)}{E}\frac{6(1+\nu)}{5} c\tan(\alpha-\gamma)\ln\left(\frac{a}{b}\right). \end{aligned} \tag{6}$$

The thread tooth deformation δ_c caused by tooth root incline can be expressed as

$$\begin{aligned} & \delta_c(x) \\ & = \frac{N(x)\cos(\alpha-\gamma)}{E}\frac{12c(1-\nu^2)}{\pi a^2}\left[c - \frac{b}{2}\tan(\alpha-\gamma)\right]. \end{aligned} \tag{7}$$

The thread tooth deformation δ_d caused by shear deformation of tooth root can be expressed as

$$\begin{aligned} \delta_d(x) = {} & \frac{N(x)\cos(\alpha-\gamma)}{E}\frac{2(1-\nu^2)}{\pi} \\ & \cdot \left[\frac{P}{a}\ln\left(\frac{P+0.5a}{P-0.5a}\right) + \frac{1}{2}\ln\left(4\frac{P^2}{a^2} - 1\right)\right]. \end{aligned} \tag{8}$$

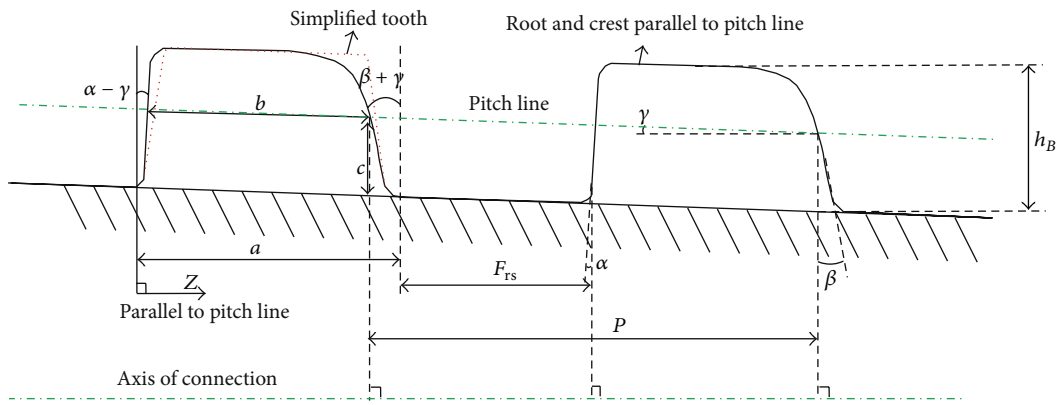

Figure 3: The schematic of simplified cantilever beam model of an isosceles trapezoid for buttress type thread tooth.

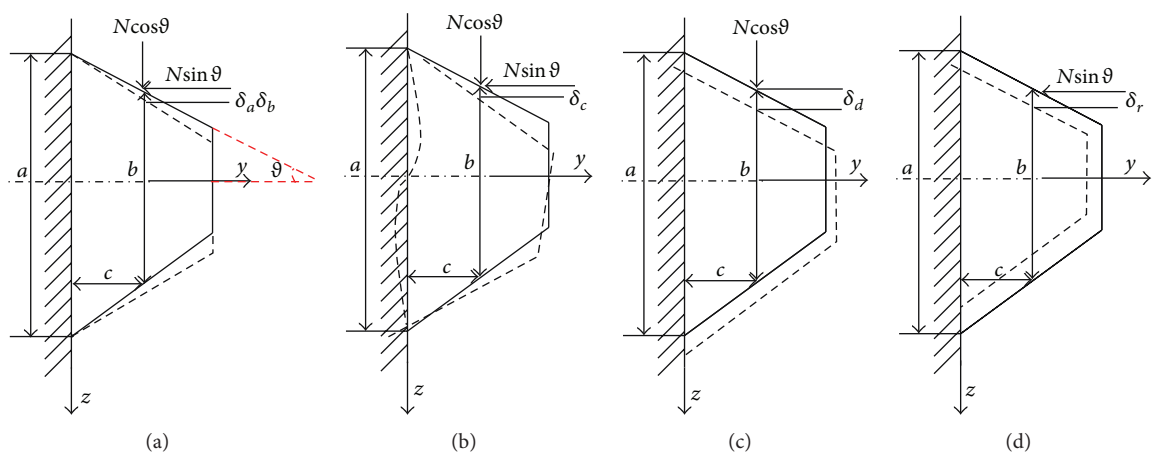

Figure 4: The elastic deformations of simplified thread tooth (a) deformation caused by tooth bending or shear force; (b) deformation caused by tooth root incline; (c) deformation caused by shear deformation of tooth root; (d) deformation caused by radial effect.

The deformations δ_{rp}, δ_{rc} caused by radial effect for pin thread tooth and coupling thread tooth can be, respectively, expressed as

$$\delta_{rp}(x) = \frac{N(x)\cos(\alpha-\gamma)}{E}\frac{\tan^2(\alpha-\gamma)}{2P} \cdot \left[\frac{d_2^2(x)+4r_0^2}{d_2^2(x)-4r_0^2} - \nu\right] d_2(x), \tag{9}$$

$$\delta_{rc}(x) = \frac{N(x)\cos(\alpha-\gamma)}{E}\frac{\tan^2(\alpha-\gamma)}{2P} \cdot \left(\frac{4R_0^2+d_2^2(x)}{4R_0^2-d_2^2(x)} - \nu\right) d_2(x). \tag{10}$$

Consequently, the total elastic deformations δ_{tp}, δ_{tc} for pin thread tooth and coupling thread tooth along its cone direction (Z direction) are, respectively, as follows:

$$\delta_{tp}(x) = \delta_a + \delta_b + \delta_c + \delta_d + \delta_{rp} = \frac{[k + k_{rp}(x)]\, N(x)\cos(\alpha-\gamma)}{E}, \tag{11}$$

$$\delta_{tc}(x) = \delta_a + \delta_b + \delta_c + \delta_d + \delta_{rc} = \frac{[k + k_{rc}(x)]\, N(x)\cos(\alpha-\gamma)}{E}. \tag{12}$$

In (11) and (12), $k = k_a + k_b + k_c + k_d$. The deformation coefficients k_a, k_b, k_c, k_d, k_{rp}, and k_{rc} can be determined from (5) to (10).

In (5)~(12), $N(x)$ denotes the normal load acting on the load flank of thread tooth within unit axial length dx. Because the load flank angle and thread taper are both very small in premium threaded connection, we ignored the axial components of frictional force on load flank and that of the contact stress between root and crest. The relation between $N(x)$ and $f(x)$ can be briefly expressed as

$$N(x)\frac{\cos\alpha}{\tan[\psi(x)]}\mathrm{d}x = f(x)\,\mathrm{d}x. \tag{13}$$

In (13), the helix angle $\psi(x)$ is

$$\psi(x) = \arctan\left[\frac{P}{\pi d_2(x)}\right], \quad d_2(x) = d_{2s} - 2x\tan\gamma. \tag{14}$$

By submitting (1) and (14) into (13), we can get

$$N(x) = \frac{P}{\pi d_2(x)\cos\alpha}\frac{\mathrm{d}F(x)}{\mathrm{d}x}. \tag{15}$$

Then, by submitting (15) into (11) and (12), the total elastic deformations for pin thread tooth and coupling thread tooth are, respectively, as follows:

$$\begin{aligned}\delta_{\mathrm{tp}}(x) &= \lambda_{\mathrm{p}}(x)\frac{\mathrm{d}F(x)}{\mathrm{d}x}\\ &= \frac{\left[k+k_{\mathrm{rp}}(x)\right]}{E}\frac{\cos(\alpha-\gamma)}{\cos\alpha}\frac{P}{\pi d_2(x)}\frac{\mathrm{d}F(x)}{\mathrm{d}x},\end{aligned} \tag{16}$$

$$\begin{aligned}\delta_{\mathrm{tc}}(x) &= \lambda_{\mathrm{c}}(x)\frac{\mathrm{d}F(x)}{\mathrm{d}x}\\ &= \frac{\left[k+k_{\mathrm{rc}}(x)\right]}{E}\frac{\cos(\alpha-\gamma)}{\cos\alpha}\frac{P}{\pi d_2(x)}\frac{\mathrm{d}F(x)}{\mathrm{d}x}.\end{aligned} \tag{17}$$

In (16) and (17), the coefficients λ_{p} and λ_{c} depend on the geometry parameters of connection and thread tooth as well as the used material properties, whose derivatives for x are, respectively, as follows:

$$\begin{aligned}\lambda_{\mathrm{p}}' &= \frac{\mathrm{d}\lambda_{\mathrm{p}}}{\mathrm{d}x} = \frac{\cos(\alpha-\gamma)}{E\cos\alpha}\frac{\mathrm{d}\left[\left(k+k_{\mathrm{rp}}\right)(P/\pi d_2)\right]}{\mathrm{d}x}\\ &= \frac{\cos(\alpha-\gamma)}{E\cos\alpha}\left[\frac{\mathrm{d}\left(k+k_{\mathrm{rp}}\right)}{\mathrm{d}x}\frac{P}{\pi d_2}+\left(k+k_{\mathrm{rp}}\right)\frac{\mathrm{d}(P/\pi d_2)}{\mathrm{d}x}\right]\\ &= \frac{\cos(\alpha-\gamma)}{E\cos\alpha}\left\{\frac{\tan^2(\alpha-\gamma)\tan\gamma}{P}\right.\\ &\qquad\cdot\left[\frac{d_2^2+4r_0^2}{d_2^2-4r_0^2}-\frac{16d_2^2r_0^2}{\left(d_2^2-4r_0^2\right)^2}-\nu\right]\\ &\qquad\left.\cdot\frac{P}{\pi d_2}-\left(k+k_{\mathrm{rp}}\right)\frac{2P\tan\gamma}{\pi d_2^2}\right\}\\ &= \frac{\tan\gamma\cos(\alpha-\gamma)}{\pi E d_2(x)\cos\alpha}\left\{\tan^2(\alpha-\gamma)\right.\\ &\qquad\cdot\left[\frac{d_2^4(x)-16r_0^4-16r_0^2d_2^2(x)}{\left(d_2^2(x)-4r_0^2\right)^2}-\nu\right]\\ &\qquad\left.-\left(k+k_{\mathrm{rp}}\right)\frac{2P}{d_2(x)}\right\},\end{aligned} \tag{18}$$

$$\begin{aligned}\lambda_{\mathrm{c}}' &= \frac{\mathrm{d}\lambda_{\mathrm{c}}}{\mathrm{d}x} = \frac{\cos(\alpha-\gamma)}{E\cos\alpha}\frac{\mathrm{d}\left[\left(k+k_{\mathrm{rc}}\right)(P/\pi d_2)\right]}{\mathrm{d}x}\\ &= \frac{\cos(\alpha-\gamma)}{E\cos\alpha}\left[\frac{\mathrm{d}\left(k+k_{\mathrm{rc}}\right)}{\mathrm{d}x}\frac{P}{\pi d_2}+\left(k+k_{\mathrm{rc}}\right)\frac{\mathrm{d}(P/\pi d_2)}{\mathrm{d}x}\right]\\ &= \frac{\cos(\alpha-\gamma)}{E\cos\alpha}\left\{\frac{\tan^2(\alpha-\gamma)\tan\gamma}{P}\right.\\ &\qquad\cdot\left[\frac{4R_0^2+d_2^2}{4R_0^2-d_2^2}+\frac{16R_0^2d_2^2}{\left(4R_0^2-d_2^2\right)^2}-\nu\right]\\ &\qquad\left.\cdot\frac{P}{\pi d_2}-\left(k+k_{\mathrm{rc}}\right)\frac{2P\tan\gamma}{\pi d_2^2}\right\}\\ &= \frac{\tan\gamma\cos(\alpha-\gamma)}{\pi E d_2(x)\cos\alpha}\left\{\tan^2(\alpha-\gamma)\right.\\ &\qquad\cdot\left[\frac{16R_0^4-d_2^4(x)+16R_0^2d_2^2(x)}{\left(4R_0^2-d_2^2(x)\right)^2}-\nu\right]\\ &\qquad\left.-\left(k+k_{\mathrm{rc}}\right)\frac{2P}{d_2(x)}\right\}.\end{aligned} \tag{19}$$

2.3. Differential Equation of the Axial Load $F(x)$. Under the action of pretightening force, the pin thread and coupling thread are always engaged to each other, indicating that their thread pitches are equal after deformation. However, the compressed pin will make its own thread pitch decrease while the stretched coupling will make its own thread pitch increase. The deformation of pin thread tooth should increase its own pitch while the deformation of coupling thread tooth should reduce its own pitch, thus guaranteeing the equal pitch and the perfectly engaged state for pin thread and coupling thread.

According to Hooke's law, the compressed and stretched elastic deformations of pin and coupling body along the thread cone direction are, respectively, as follows:

$$\chi_{\mathrm{p}} = \frac{4}{\pi E\cos\gamma}\int_0^x\frac{F(x)}{\left[d_2(x)-h_B\right]^2-4r_0^2}\mathrm{d}x, \tag{20}$$

$$\chi_{\mathrm{c}} = \frac{4}{\pi E\cos\gamma}\int_0^x\frac{F(x)}{4R_0^2-\left[d_2(x)+h_B\right]^2}\mathrm{d}x. \tag{21}$$

Moreover, the deformation compatibility equation can be obtained from the equal pitch after deformation for pin thread and coupling thread:

$$\begin{aligned}\chi_{\mathrm{p}}(x)+\chi_{\mathrm{c}}(x) &= \left[\delta_{\mathrm{tp}}(x)+\delta_{\mathrm{tc}}(x)\right]\\ &\quad-\left[\delta_{\mathrm{tp}}(0)+\delta_{\mathrm{tc}}(0)\right].\end{aligned} \tag{22}$$

Then, by submitting (16), (17), (20), and (21) into (22), we get

$$\frac{4}{\pi E\cos\gamma}\left\{\int_0^x\left[\frac{1}{\left[d_2(x)-h_B\right]^2-4r_0^2}+\frac{1}{4R_0^2-\left[d_2(x)+h_B\right]^2}\right]F(x)\,\mathrm{d}x\right\}=\left(\lambda_{\mathrm{p}}+\lambda_{\mathrm{c}}\right)\frac{\mathrm{d}F(x)}{\mathrm{d}x}. \tag{23}$$

Taking the derivative with respect to x for (23) and considering that $\lambda_{\mathrm{p}}+\lambda_{\mathrm{c}}\neq 0$, the differential equation of axial load distribution can be obtained as

$$\begin{aligned}&\frac{\mathrm{d}^2F(x)}{\mathrm{d}x^2}+m(x)\frac{\mathrm{d}F(x)}{\mathrm{d}x}+n(x)F(x)=0,\\&m(x)=\left(\frac{\lambda_{\mathrm{p}}'+\lambda_{\mathrm{c}}'}{\lambda_{\mathrm{p}}+\lambda_{\mathrm{c}}}\right),\\&n(x)=-\frac{4}{\pi E\left(\lambda_{\mathrm{p}}+\lambda_{\mathrm{c}}\right)\cos\gamma}\cdot\left\{\frac{1}{\left[d_2(x)-h_B\right]^2-4r_0^2}+\frac{1}{4R_0^2-\left[d_2(x)+h_B\right]^2}\right\}.\end{aligned} \tag{24}$$

The boundary conditions for (24) are

$$\begin{aligned}F(0)&=0,\\F(L)&=F_t.\end{aligned} \tag{25}$$

2.4. Solution of Differential Equation. The axial load distribution equation (24) is a nonlinear differential equation and its analytical solution is very difficult to get, so we solved its numerical solution with finite difference method. First, we divided the engaged thread according to unit length of thread pitch P and numbered the node $0\sim N_t$ successively from the big end of the pin thread, so the coordinate for node i was $x_i=iP$. Then we took F_i to denote the node force $F(x_i)$ and considered the boundary conditions equation (25). Finally, the difference equation of (24) can be obtained as

$$A\left[F_1\ \ F_2\ \ \cdots\ \ F_{N-1}\right]^{\mathrm{T}}=B. \tag{26}$$

In (26), the coefficient matrix is

$$A=\begin{bmatrix}-\frac{2}{P^2}+n(x_1) & \frac{1}{P^2}+\frac{m(x_1)}{2P} & & & 0\\ \frac{1}{P^2}-\frac{m(x_2)}{2P} & -\frac{2}{P^2}+n(x_2) & \frac{1}{P^2}+\frac{m(x_2)}{2P} & & \\ \cdots & \frac{1}{P^2}-\frac{m(x_i)}{2P} & -\frac{2}{P^2}+n(x_i) & \frac{1}{P^2}+\frac{m(x_i)}{2P} & \cdots\\ & & \cdots & & \\ 0 & & & \frac{1}{P^2}-\frac{m(x_{N-1})}{2P} & -\frac{2}{P^2}+n(x_{N-1})\end{bmatrix}. \tag{27}$$

And the constant term column matrix is

$$B=\left[0\ \ 0\ \ \cdots\ \ -\left(\frac{1}{P^2}+\frac{m(x_{N-1})}{2P}\right)F_t\right]^{\mathrm{T}}. \tag{28}$$

The difference equation (26) was solved based on Gaussian main elimination method.

2.5. Geometric Description for Load Flank of Thread Tooth. For calculating the mean contact stress on the load flank of thread tooth, the geometric description of thread surface is necessary. Setting the premium thread connection as the x-axis and its intersection with the plane of thread load flank as the origin, we established global coordinate system O-xyz, whose unit vectors are **i**, **j**, and **k**, respectively, shown in Figure 5.

For determining the unit normal vector **n** and unit tangent vector $\boldsymbol{\tau}$ of thread surface, the cylindrical coordinate system O-$r\vartheta x$ was also established and its vectors are

$$\begin{aligned}\mathbf{u}&=-\mathbf{j},\\\mathbf{v}&=-\mathbf{k},\\\mathbf{w}&=\mathbf{i}.\end{aligned} \tag{29}$$

The plane $OB_2C_2D_2$, which stands for thread load flank, can be obtained by rotating the quadrangle $OBCD$ in yoz plane α around the y-axis and then ψ around the z-axis successively. If quadrangle $OBCD$ is a 1×1 square, its

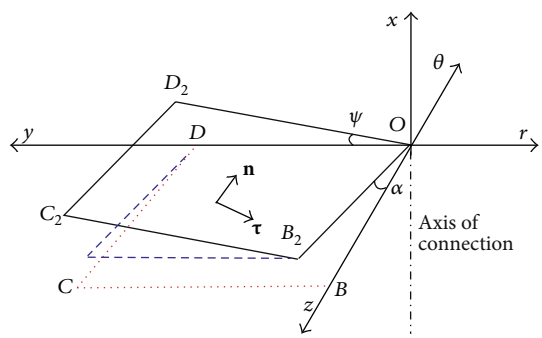

FIGURE 5: Geometric description schematic of thread load flank.

vertices after 2 rotations are $O(0, 0, 0)$, $B_2(\sin\alpha, 0, \cos\alpha)$, $C_2(\sin\alpha + \sin\psi, \cos\psi, \cos\alpha)$, and $D_2(\sin\psi, \cos\psi, 0)$. Thus, the equation of load flank plane can be obtained as

$$x - y\tan\psi - z\tan\alpha = 0. \tag{30}$$

The unit normal vector $\mathbf{n}$ and unit tangent vector $\boldsymbol{\tau}$ of thread load flank are

$$\mathbf{n} = \frac{\mathbf{i} - \tan\psi\mathbf{j} - \tan\alpha\mathbf{k}}{\sqrt{1 + \tan^2\psi + \tan^2\alpha}} = \frac{\tan\psi\mathbf{u} + \tan\alpha\mathbf{v} + \mathbf{w}}{\sqrt{1 + \tan^2\psi + \tan^2\alpha}},$$
$$\boldsymbol{\tau} = -\sin\psi\mathbf{i} - \cos\psi\mathbf{j} = \cos\psi\mathbf{u} - \sin\psi\mathbf{w}. \tag{31}$$

And the infinitesimal area of thread surface $\mathrm{d}\Omega$ can be also expressed with the infinitesimal area $\mathrm{d}A$ in the axial cross section as

$$\mathrm{d}\Omega = \sqrt{1 + \tan^2\psi + \tan^2\alpha}\,\mathrm{d}A. \tag{32}$$

2.6. Mean Contact Stress on Load Flank of Thread Tooth. Supposing that the contact stress on load flank was uniform and that the helix angle was constant in each engaged thread, the axial component of contact stress integral on the load flank within each engaged thread should be equal to the axial load acting on itself; that is,

$$\iint_{\Omega_i} \left[\left(p_i\mathbf{n}_i + \mu_t p_i\boldsymbol{\tau}_i\right)\mathrm{d}\Omega\right]\cdot\mathbf{i} = F_{iP}. \tag{33}$$

By submitting (31) and (32) into (33), the mean contact stress on load flank of ith tooth is

$$p_i = \frac{F_{iP}}{\left(1 - \mu_t\sqrt{1 + \tan^2\psi_i + \tan^2\alpha}\sin\psi_i\right)\iint_{A_i}\mathrm{d}A}. \tag{34}$$

In (34),

$$\iint_{A_i}\mathrm{d}A = \int_0^{2\pi}\int_{\{d_2[(i-1)P]-\vartheta(p\tan\gamma)/\pi-h_B\}/2}^{\{d_2[(i-1)P]-\vartheta(p\tan\gamma)/\pi+h_B\}/2} r\,\mathrm{d}r\,\mathrm{d}\vartheta$$
$$= \pi h_B\left[d_{2s} - (2i+1)P\tan\gamma\right]. \tag{35}$$

At last, the mean contact stress on the load flank of ith tooth is

$$p_i = F_{iP}\left(\pi h_B\left(1 - \mu_t\sqrt{1 + \tan^2\psi_i + \tan^2\alpha}\sin\psi_i\right)\cdot\left[d_{2s} - (2i+1)P\tan\gamma\right]\right)^{-1}. \tag{36}$$

3. Calculation Example

3.1. Analytical Method. For simplicity, the geometrical parameters of a premium connection are mainly taken from API 177.8 mm, P110 grade, buttress thread casing in API Spec.5B. Its geometry parameters and material properties are listed in Table 1.

Suppose the pretightening force F_t from sealing surface and shoulder contact is 1000 KN; the axial load acting on each engaged thread F_{iP} and the mean contact stress on load flank p_i can be calculated according to the analytical model proposed in this paper; the results are shown in Figures 6 and 7, respectively.

Figure 6 shows that the load acting on engaged thread tooth increases with the increase of thread number and that the last 4~6 engaged threads bear more than 90% of the pretightening force. Particularly for the last engaged thread, it carries 44.54% of the pretightening force. The load distribution is similar to the practical situation in threaded connection, indicating that the proposed analytical method is reasonable. Meanwhile, contact stress distribution on load flank of thread teeth shows a similar pattern to the load distribution, whose maximum value is 522.74 MPa on the last engaged thread, shown in Figure 7. It is obvious that thread surface would sustain a galling risk if the pretightening force is increased to some extent.

3.2. Finite Element Method. In order to validate the proposed analytical model in this paper, we analyzed the same sample with the finite element software ANSYS 14.5. Considering the characteristics of axisymmetric load and boundary conditions, a 2D finite element model of modified API 177.8 mm premium thread connection has been established (shown in Figure 8).

To make the simulated results more approachable to practical situations, the materials of pin and coupling were both defined as bilinear isotropic hardening model in the FEM. The frictional contact type between pin thread and coupling thread has been selected, indicating that the contact between thread teeth is taken as an elastic-plastic and frictional contact problem. The eight-node quadrilateral element Quad 8 node-183, which can be used as an axisymmetric element to simulate plastic deformation, was selected for this analysis. The element size was controlled and then local mesh refinement was applied to the thread tooth edges. Figures 9 and 10 show the mesh on the whole model and the teeth edges. Because the contact between engaged thread teeth is a material and boundary nonlinear problem, static analysis has been selected for solving it. The boundary conditions set for

Table 1: Geometry parameters and material properties of premium connection.

Symbol	Value	Unit	Symbol	Value	Unit
R_0	98	mm	F_{rs}	2.39	mm
r_0	78.54	mm	h_B	1.58	mm
P	5.08	mm	N_t	15	Integer
d_{2s}	176.63	mm	E	206	GPa
γ	1.79	Degree	ν	0.3	Dimensionless
α	3	Degree	μ_t	0.08	Dimensionless
β	10	Degree	f_{ymn}	758.42	MPa

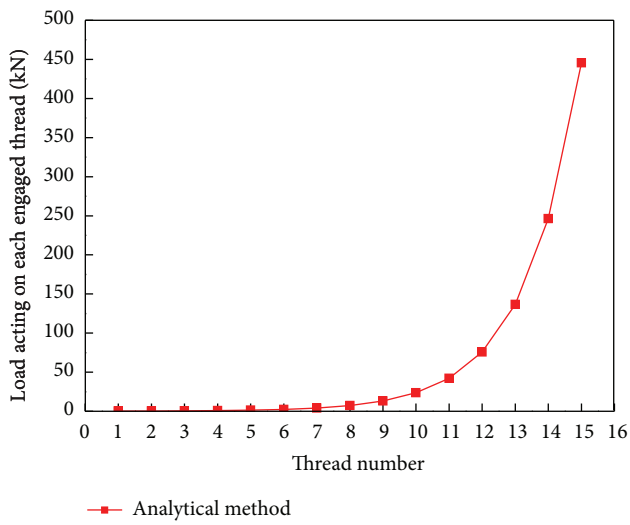

Figure 6: Load acting on each engaged thread by the proposed analytical model.

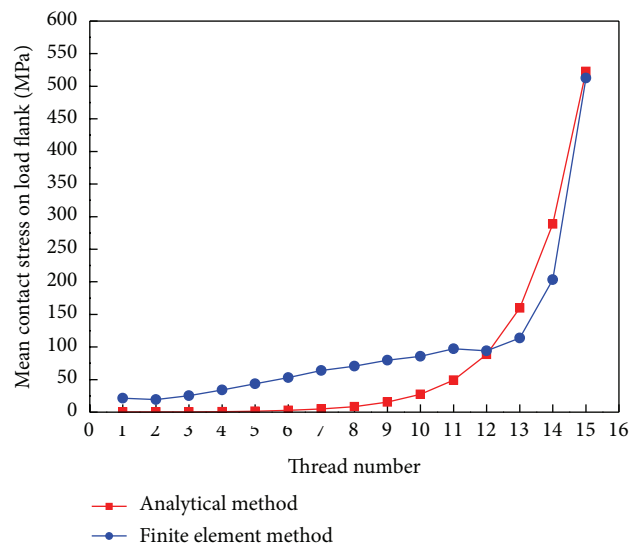

Figure 7: Mean contact stress on load flank of thread tooth in premium connection obtained by analytical method and finite element method.

this analysis are an axial displacement confined at the big end of coupling thread and application of 313.93 MPa compressed stress, which is equivalent to 1000 KN of pretightening force, on the small end of pin thread. By using ANSYS, we can acquire the stress distribution on the thread teeth (shown in Figure 11).

Figure 11 shows the Von-Mises stress distribution on each contact thread tooth. In Figure 11, we can find that the last 4~6 engaged threads bear almost all the pretightening force, which is identical to the load distribution calculated by the proposed analytical model in this paper.

3.3. Comparison and Discussion. The mean contact stress on the load flank of thread teeth calculated from the proposed analytical model and that obtained by FEM are compared in Figure 7. One can find that both curves are identical in trend and that the minimum and maximum values obtained by the proposed analytical method are also close to those of FEM. Meanwhile, we can also find that there exists some discrepancy in the middle region of the two curves, which may be attributed to the simplifications and assumptions of the analytical model. The helix angle in the analytical model may be a reason because the 2D FEM cannot contain this factor. However, the analytical model can still predict a relatively meaningful stress value for the last engaged threads, which is the easiest one to fail.

Figure 12 shows the comparison of mean contact stresses on the last engaged threads under different pretightening forces. It can be seen from Figure 12 that mean contact stress on the last engaged thread obtained by analytical model keeps increasing linearly with the increase of pretightening force, while that calculated from FEM tends to be stable after a section of linear increase. This discrepancy can mainly because that elastic deformation has been supposed for the analytical model but elastic-plastic deformation considered in FEM. Because the allowable in-service pretightening force is about 1350 KN~1750 KN, the error of the analytical model for the stress on the last engaged thread is about 6.2%~18.1%. Consequently, the proposed analytical method has certain accuracy and can, to some extent, meet the needs of engineering.

4. Conclusions

(1) This paper proposes an analytical model for investigating loading and contact stress on the thread teeth

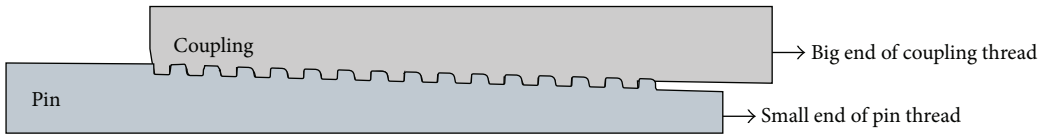

Figure 8: Finite element model of modified API 177.8 mm premium connection.

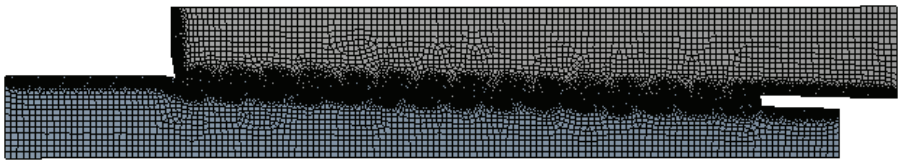

Figure 9: Mesh on the whole finite element model.

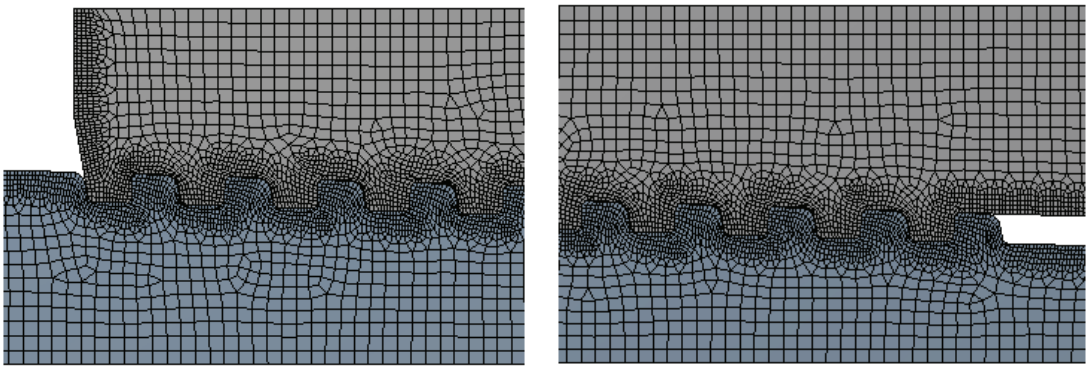

(a) (b)

Figure 10: Refined mesh at teeth edges: (a) left region and (b) right region.

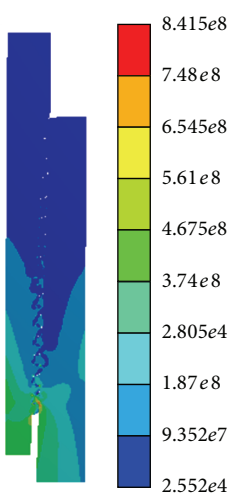

Figure 11: Von-Mises stress distribution on the thread teeth in ANSYS.

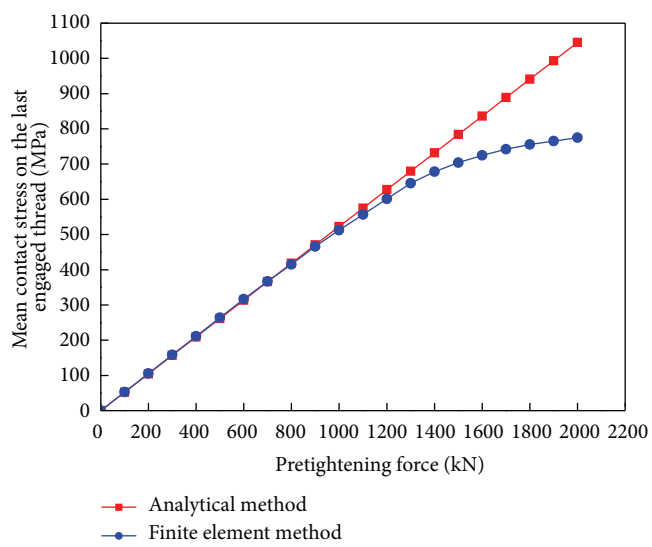

Figure 12: Comparison of mean contact stresses on the last engaged thread tooth under different pretightening forces.

in tubing and casing premium threaded connection on the basis of elastic mechanics.

(2) The proposed analytical model is validated by the application of the FEM to the same sample. The pretightening force mainly applies to the last 4~6 engaged threads, about 50% of that to the last engaged threads.

(3) Comparing the contact stress of the last engaged thread between the analytical model and FEM shows that the accuracy of the analytical model will decline with the increase of pretightening force after the material enters into plastic deformation. In practice, the relative error is about 6.2%~18.1%. This indicates that the analytical method can, to some extent, meet the needs of engineering.

Nomenclature

F_t: Total force transferred by engaged threads
N_t: Total number of engaged thread teeth
$N(x)$: Normal load acting on the load flank of thread tooth within unit axial length dx
$f(x)$: Axial load distribution intensity
$F(x)$: Axial load distribution
F_{iP}: Axial load acted on each engaged thread
P: Pitch of thread
α: Load flank angle in the axial cross section of thread
β: Leading flank angle in the axial cross section of thread
$\psi(x)$: Helix angle
$d_2(x)$: Pitch diameter
d_{2s}: Pitch diameter at the big end of pin thread
γ: Half angle of thread cone
a: Root width of isosceles trapezoid tooth
b: The width of isosceles trapezoid tooth at pitch diameter
c: The distance from pitch diameter of isosceles trapezoid tooth to its root
F_{rs}: Root width of buttress type tooth
h_B: Completed thread height
δ_{tp}: Total elastic compressed deformation of pin thread tooth
δ_{tc}: Total elastic stretched deformation of coupling thread tooth
$\delta_a, \delta_b, \delta_c, \delta_d$: Elastic deformation of thread tooth caused by tooth bending, shear force, root incline, and shear deformation of tooth root, respectively
$\delta_{\mathrm{rp}}, \delta_{\mathrm{rc}}$: Elastic deformation of thread tooth caused by radial effect for pin thread tooth and coupling thread tooth, respectively
$k_a, k_b, k_c, k_d, k_{\mathrm{rp}}, k_{\mathrm{rc}}, k, \lambda_{\mathrm{p}}, \lambda_{\mathrm{c}}$: Relevant deformation coefficients of thread tooth
E: Elastic modulus of material
ν: Poisson ratio of material
f_{ymn}: Specified minimum yield strength of material
r_0: Internal radius of pipe
R_0: External radius of coupling
$\chi_{\mathrm{p}}, \chi_{\mathrm{c}}$: Compressed and stretched elastic deformation along thread cone direction for pipe and coupling body, respectively
m, n: Coefficients of differential equation
F_i: Axial load on ith node
p_i: Mean contact stress on the load flank of ith tooth
μ_t: Frictional coefficient on the thread surface
ψ_i: Mean helix angle on ith tooth.

Conflict of Interests

The authors declare that there is no conflict of interests regarding the publication of this paper.

Acknowledgments

The authors are grateful for the support of the National Natural Science Foundation of China (Grant nos. 50904050 and 51244007) and the financial support of Tianjin Pipe (Group) Co., Ltd.

References

[1] G. Carcagno, "The design of tubing and casing premium connections for HTHP wells," in *Proceedings of the SPE High Pressure/High Temperature Sour Well Design Applied Technology Workshop*, Society of Petroleum Engineers, 2005.

[2] A. Bradley, S. Nagasaku, and E. Verger, "Premium connection design testing and installation for HPHT sour wells," in *SPE High Pressure/High Temperature Sour Well Design Applied Technology Workshop*, Society of Petroleum Engineers, 2005.

[3] M. Sugino, K. Nakamura, S. Yamaguchi, D. Daly, G. Briquet, and E. Verger, "Development of an innovative high-performance premium threaded connection for OCTG," in *Proceedings of the Offshore Technology Conference (OTC '10)*, pp. 1883–1891, May 2010.

[4] L. Maduschka, "Beanspruchung von Schraubenverbindungen und zweckmäßige Gestaltung der Gewindeträger," *Forschung auf dem Gebiete des Ingenieurwesens A*, vol. 7, no. 6, pp. 299–305, 1936.

[5] D. Sopwith, "The distribution of load in screw threads," *Proceedings of the Institution of Mechanical Engineers*, vol. 159, no. 1, pp. 373–383, 1948.

[6] S. Yazawa and K. Hongo, "Distribution of load in the screw thread of a bolt-nut connection subjected to tangential forces and bending moments," *JSME International Journal I, Solid Mechanics, Strength of Materials*, vol. 31, no. 2, pp. 174–180, 1988.

[7] W. Wang and K. M. Marshek, "Determination of the load distribution in a threaded connector having dissimilar materials and varying thread stiffness," *Journal of Engineering for Industry*, vol. 117, no. 1, pp. 1–8, 1995.

[8] L. Bruschelli and V. Latorrata, "The influence of "shell behavior" on load distribution for thin-walled conical joints," *Journal of Applied Mechanics*, vol. 67, no. 2, pp. 298–306, 2000.

[9] S.-J. Chen, Q. An, Y. Zhang, L.-X. Gao, and Q. Li, "Loading analysis on the thread teeth in cylindrical pipe thread connection," *Journal of Pressure Vessel Technology*, vol. 132, no. 3, pp. 0312021–0312028, 2010.

[10] P. O'Hara, "Finite element analysis of threaded connections," in *Proceedings of the Army Symposium on Solid Mechanics*, DTIC Document, pp. 99–119, 1974.

[11] J. L. Bretl and R. D. Cook, "Modelling the load transfer in threaded connections by the finite element method," *International Journal for Numerical Methods in Engineering*, vol. 14, no. 9, pp. 1359–1377, 1979.

[12] H. Zhao, "A numerical method for load distribution in threaded connections," *Journal of Mechanical Design*, vol. 118, no. 2, pp. 274–279, 1996.

[13] H. Zhao, "Stress concentration factors within bolt-nut connectors under elasto-plastic deformation," *International Journal of Fatigue*, vol. 20, no. 9, pp. 651–659, 1998.

[14] K. A. Macdonald and W. F. Deans, "Stress analysis of drillstring threaded connections using the finite element method," *Engineering Failure Analysis*, vol. 2, no. 1, pp. 1–30, 1995.

[15] H. Bahai, G. Glinka, and I. I. Esat, "Numerical and experimental evaluation of SIF for threaded connectors," *Engineering Fracture Mechanics*, vol. 54, no. 6, pp. 835–845, 1996.

[16] J.-J. Chen and Y.-S. Shih, "Study of the helical effect on the thread connection by three dimensional finite element analysis," *Nuclear Engineering and Design*, vol. 191, no. 2, pp. 109–116, 1999.

[17] S. Baragetti, "Effects of taper variation on conical threaded connections load distribution," *Journal of Mechanical Design*, vol. 124, no. 2, pp. 320–329, 2002.

[18] T. Fukuoka and M. Nomura, "Proposition of helical thread modeling with accurate geometry and finite element analysis," *Journal of Pressure Vessel Technology*, vol. 130, no. 1, Article ID 011204, pp. 1–6, 2008.

[19] E. Stoeckly and H. Macke, "Effect of taper on screw thread load distribution," *Transactions of the ASME*, vol. 74, no. 1, pp. 103–112, 1952.

[20] G. Yuan, Z. Yao, J. Han, and Q. Wang, "Stress distribution of oil tubing thread connection during make and break process," *Engineering Failure Analysis*, vol. 11, no. 4, pp. 537–545, 2004.

[21] J. C. R. Plácido, P. E. Valadã de Miranda, T. A. Netto, I. P. Pasqualino, G. F. Miscow, and B. de Carvalho Pinheiro, "Fatigue analysis of aluminum drill pipes," *Materials Research*, vol. 8, no. 4, pp. 409–415, 2005.

[22] M. Slack, H. Salkin, and F. Langer, "Technique to assess directly make-up contact stress inside tubular connections," in *SPE/IADC Drilling Conference*, Society of Petroleum Engineers, 1990.

[23] K. A. Hamilton, B. Wagg, and T. Roth, "Using ultrasonic techniques to accurately examine seal surface contact stress in premium connections," in *Proceedings of the SPE Annual Technical Conference and Exhibition*, pp. 3461–3471, Society of Petroleum Engineers, November 2007.

[24] A. Yamamoto, *The Theory and Computation of Thread Connection*, Youkendo, Tokyo, Japan, 1980, (Japanese).

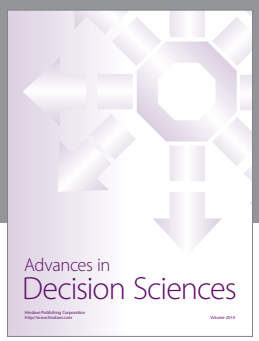

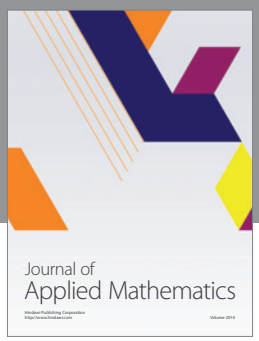

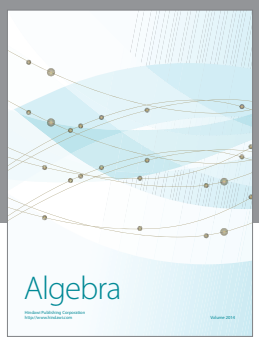

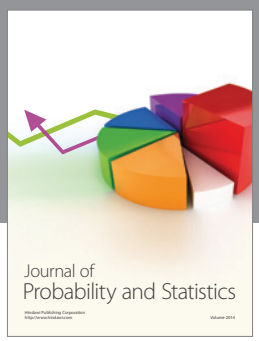

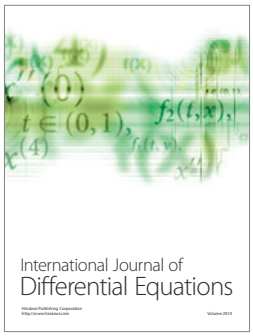

Hindawi
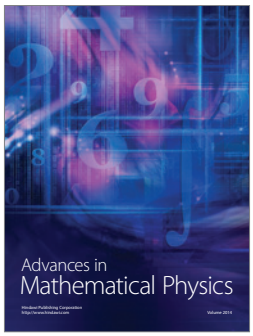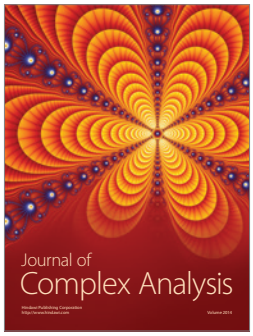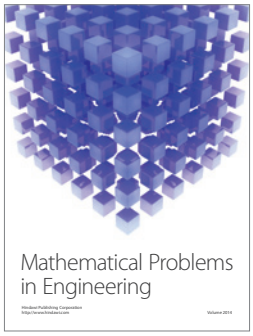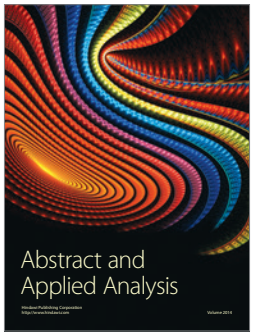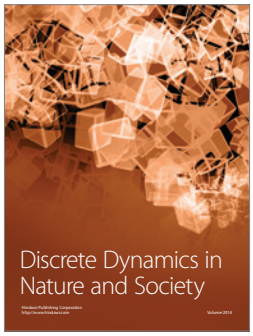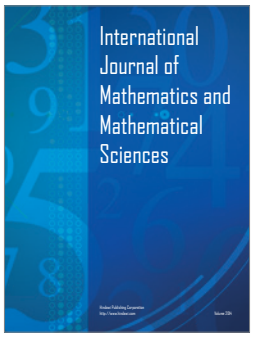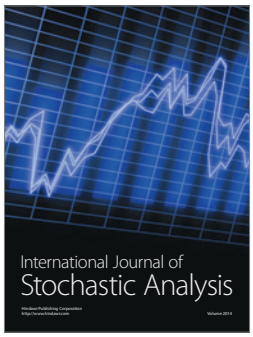
Submit your manuscripts at
http://www.hindawi.com